Interlayer coupling in rotationally faulted multilayer graphenes

E. J. Mele

Department of Physics and Astronomy
David Rittenhouse Laboratory
University of Pennsylvania
Philadelphia, PA 19104

Abstract. This article reviews progress in the theoretical modelling of the electronic structure of rotationally faulted multilayer graphenes. In these systems the crystallographic axes of neighboring layers are misaligned so that the layer stacking does not occur in the Bernal structure observed in three dimensional graphite and frequently found in exfoliated bilayer graphene. Notably, rotationally faulted graphenes are commonly found in other forms of multilayer graphene including epitaxial graphenes thermally grown on SiC $(000\bar{1})$, graphenes grown by chemical vapor deposition, folded mechanically exfoliated graphenes, and graphene flakes deposited on graphite. Rotational faults are experimentally associated with a strong reduction of the energy scale for coherent single particle interlayer motion. The microscopic basis for this reduction and its consequences have attracted significant theoretical attention from several groups that are highlighted in this review.

1. Introduction

Coherent interlayer motion in multilayer graphenes play a crucial role in determining their low energy electronic properties. In single layer graphene the absence of the layer degree of freedom cleanly exposes the geometrical structure of its low energy electronic physics. This is controlled by single particle spectra containing linearly dispersing bands around singular points at its inequivalent zone corners, described by a pair of valley-polarized two dimensional massless Dirac Hamiltonians [1, 2]. The physics is very different for graphene bilayers that are stacked in the Bernal geometry with the "A" sublattice of one layer eclipsed with the "B" sublattice of its neighbor (AB stacking). Here the effects of coherent interlayer coupling are quite strong and the low energy sector is described instead by a *different* class layer-coherent chiral fermions with a quadratic dispersion and a Berry's phase of 2π for reciprocal space orbits that encircle the point of degeneracy [3]. This physics is readily understood from the experimentally known strength of the interlayer tunneling amplitude at eclipsed sites and it can be generalized to describe the low energy physics of multi-layer graphenes where the crystallographic axes of neighboring layers are rotated by special angles $\theta = n\pi/3$ [4, 5, 6, 7].

Surprisingly, experimental work over the last five years has revealed a family of multilayer graphenes that show only weak (if any) effects of their interlayer coupling. This family includes graphenes that are grown epitaxially on the $\mathrm{SiC\,(000\bar{1})}$ surface [8, 9, 10], CVD grown graphenes [11] and some forms of exfoliated graphene [12, 13, 14]. A common structural attribute of these systems is a rotational misorientation (a twist) of their neighboring layers at angles of $\theta \neq n\pi/3$. The layer decoupling has been inferred from the measurements of the magnetotransport [8, 9], of the Landau level spectra observed in scanning tunneling spectroscopy [14, 15] and perhaps most clearly in angle-resolved photoemission spectra [16].

These experimental observations are attracting significant theoretical attention. The layer decoupling in twisted multilayers is frequently attributed to a kinematical effect whereby the layer projections of the zone corner crystal momenta are *misaligned* by the rotation, preventing momentum-conserving interlayer motion at sufficiently low energy [17]. In this scenario the low energy theory is described by four separate valley- and layer- polarized Dirac cones. These fermions are then re-coupled at a crossover energy scale where the individual Dirac cones merge and hybridize thus changing the band topology [18]. The simplest version of this theory predicts that the residual low energy effect of the twist is to reduce the Fermi velocities by an angle dependent factor where the smallest velocities are expected for small rotation angles. These theoretical predictions have provided a taking off point for further investigations of this problem using a variety of methods ranging from microscopic atomistic calculations to continuum models designed to capture selected elements of the microscopic physics. Presently there is a lively discussion concerning the theoretical interpretation of the electronic physics in twisted graphenes: What is the appropriate long wavelength theory? How can one distinguish between the electronic physics for "small" and "large" rotation

angles? How does the the interlayer coherence scale depend on the fault angle? What are the experimental consequences of the weak interlayer coherence? It is fair to say that the one-electron physics of these systems is proving to be unexpectedly rich and it has so far eluded a satisfactory (or at least complete) theoretical description. In this article we briefly highlight some recent theoretical progress on this problem and focus on some of the major unresolved issues.

Section 2 presents a discussion of the geometric properties of rotationally faulted bilayers which are generally useful for analyzing their structural and electronic properties. The results presented here provide a foundation for a theoretical analysis we have presented earlier [19] though these details have not been published previously. Sections 3-5 briefly review the existing theoretical approaches that have been developed for describing the electronic structure of these systems. Section 3 reviews the essential features of a long wavelength theory of layer that illustrates the physics of layer decoupling by "rotational mismatch" [17]. Section 4 presents some highlights of microscopic atomistic calculations on these systems and Section 5 briefly reviews the content of several "second generation" continuum theories that refine the original theoretical proposal. Section 6 summarizes with a discussion of the connections of these theories to experiment and points to some interesting open problems.

2. Geometrical Considerations

2.1. Lattice Structures

A twisted graphene bilayer can be characterized by a relative rotation of the symmetry axes of its two layers through angle θ and a rigid translation $\vec{\Delta}$. Holding one layer fixed, a rotation about the point $\vec{r}_0$ maps coordinates $\vec{r}$ in the fixed layer to positions $\vec{r}'$ in the rotated layer in the manner

$$\vec{r}' = \mathcal{R}(\theta) \cdot (\vec{r} - \vec{r}_0) + \vec{\Delta} \tag{1}$$

where $\mathcal{R}(\theta)$ is the two-dimensional rotation operator. For definiteness one can consider the situation where the rotation is taken about a lattice site and the relative shift $\Delta = 0$. A commensurate rotation occurs when a lattice translation of the unrotated layer $\vec{T}_{mn} = m\vec{a}_1 + n\vec{a}_2$ spanned by its two primitive layer translations $\vec{a}_1$ and $\vec{a}_2$ and the mapping of an *inequivalent* translation $\vec{T}_{m'n'}$ (in the same star) are equal. This occurs only at discrete angles θ_{mn} that can be indexed by the two integers

$$e^{i\theta_{mn}} = \frac{me^{-i\pi/6} + ne^{i\pi/6}}{ne^{-i\pi/6} + me^{i\pi/6}} \tag{2}$$

Small angle rotations have large m and $n = m + 1$. These small angle faults describe large period superlattices where the atomic registry can be regarded as evolving smoothly between widely separated regions with locally Bernal-like and AA like stacking. Complementary structures with large m and $n = 1$ correspond to small angular deviations from the 60° rotated structure. Since the combination of a 60° degree rotation and a translation by a nearest neighbor bond vector is a symmetry operation

of the honeycomb lattice, a commensurate rotation near $60°$ can be regarded as the superposition of a small angle rotation and a nonprimitive translation. The primitive translations $\vec{A}$ of a general (m,n) commensuration supercell are

$$\begin{pmatrix} \vec{A}_1 \\ \vec{A}_2 \end{pmatrix} = \begin{pmatrix} m & n \\ -n & m+n \end{pmatrix} \begin{pmatrix} \vec{a}_1 \\ \vec{a}_2 \end{pmatrix} \tag{3}$$

with length $|\vec{A}| = \sqrt{m^2 + n^2 + mn}$.

Commensuration pairs at angles θ and $\bar{\theta} = 60° - \theta$ are related. The simplest example of such a pair occurs trivially for $\theta = 0$ and $\bar{\theta} = 60°$ which correspond to the smallest possible unit cells with AB (Bernal) stacking and AA (perfectly eclipsed) stacking. The unit cells of these structures have the same area but they have different sublattice symmetries. Importantly, all commensurate rotations share this property: they occur in partners where the sum of the rotation angles is $60°$ and their unit cells have the same area. The commensuration indices (m,n) and $(\bar{m},\bar{n})$ of the partners are related

$$\begin{pmatrix} \bar{m} \\ \bar{n} \end{pmatrix} = \begin{pmatrix} -1 & 1 \\ 2 & 1 \end{pmatrix} \begin{pmatrix} m \\ n \end{pmatrix} \tag{4}$$

eliminating common divisors by 3 from the result. Figure 1 illustrates this situation where the structure in the left panel corresponds to $(m,n) = (1,3)$, $\theta = 32.204°$ and on the right $(\bar{m},\bar{n}) = (2,5)$, $\bar{\theta} = 27.796°$. Partner commensurations can also be transformed into each other by a translation $\vec{\Delta}$ at a *single* rotation angle θ demonstrating the invariance of the primitive cell area. The structure at $\theta = \bar{\theta} = 30°$ is its own commensuration partner and corresponds to an elementary two dimensional quasicrystalline lattice. Note also that the form of Eqn. 1 demonstrates that the indices (m,n) generally provide a more useful specification of the structure than the fault angle θ. Indeed nearby rotation angles can have very different fault indices and therefore describe crystalline structures with vastly different periods and different physical properties. A plot of the commensuration periods $|\vec{A}|$ as a function of rotation angle θ shows a complex distribution of allowed periods which is bounded from below. This lower bound has a smooth dependence on θ, diverges as $\theta \to (0°, 30°, 60°)$ and is symmetric around the self dual state at $30°$.

Commensuration partners are distinguished by their *sublattice exchange parity*. A commensuration is sublattice exchange "even" if the commensuration cell contains an A and a B sublattice site in each layer that are coincident with atomic sites in the neighboring layer. A commensuration is sublattice exchange "odd" if only one sublattice site in the commensuration cell is eclipsed. (Fixing the rotation center of the twist at an atom site guarantees that there will be at least one coincident site.) The sublattice exchange parity can be deduced from the translation indices (m,n). It is convenient to label the eclipsed sites at the origin as the A sublattice, a nearest neighbor bond vector $\vec{\tau}$ and its partner in the rotated layer τ'. Then the condition for a second coincident site on the B sublattice is

$$\vec{T} + \vec{\tau} = \vec{T}' + \vec{\tau}' \tag{5}$$
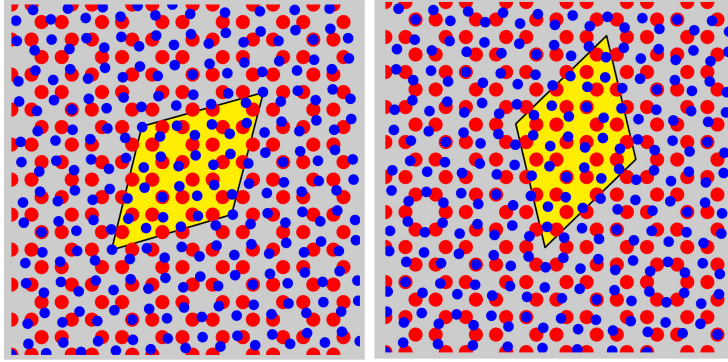
Figure 1. Two lattice structures for rotationally faulted graphene bilayers at complementary rotation angles. Red and blue dots denote atomic positions in different layers. The highlighted rhombus is a primitive commensuration cell. The figure compares the stacking patterns for commensuration pairs that are related by $\bar{\theta} = 60° - \theta$. The structures are (left) $\theta = 32.204°$ ($m = 1, n = 3$) and (right) $27.796°$ ($m = 2, n = 5$). The commensuration cells are the same for the partner structures but the point symmetry is different.

for some possible choice of $\vec{T}(\vec{T'})$ in the set of lattice translations in the reference(rotated) layers. Since the $\vec{T}$'s are both lattice translations, this requires integer (p, q) solutions to

$$e^{i\theta_{mn}} = \frac{1 + \sqrt{3}\left(pe^{i\pi/6} + qe^{-i\pi/6}\right)}{1 + \sqrt{3}\left(pe^{-i\pi/6} + qe^{i\pi/6}\right)} = \frac{me^{i\pi/6} + ne^{-i\pi/6}}{me^{-i\pi/6} + ne^{i\pi/6}} \tag{6}$$

which can be expressed

$$p = \frac{m - n + 3mq}{3n} \tag{7}$$

and has integer solutions only when $m - n$ is divisible by 3. When this is statisfied the coincident sites occur at special high symmetry points in the cell $\vec{A}_c = \pm\vec{A}_{mn}/3$ (with only one sign per structure) and correspond to high symmetry positions along the diagonal of the rhombus shown in the right hand panel of Figure 1. When $m - n$ is not divisible by 3 the only coincident site occurs at the center of rotation and its supercell translates.

2.2. Reciprocal Space

Similar considerations apply to the momentum space representation of the twisted bilayer for which Figure 2 gives a map illustrating the structure of its reciprocal space. The reciprocal lattice of the commensuration supercell can be treated as a conventional triangular lattice spanned by two primitive vectors $2\pi(\hat{e}_z \times \vec{A}_i)/\mathcal{A}$ where $\mathcal{A} = |\vec{A}_1 \times \vec{A}_2|$ is the area of the commensuration supercell and $\hat{e}_z$ is the layer normal. However, it is often useful to observe that since the real space lattice translations of the supercell
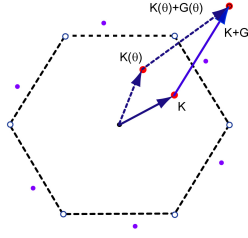
Figure 2. A reciprocal space map for a twisted graphene bilayer illustrating the rotation of the first star of reciprocal lattice vectors (open dots) to a star of rotated reciprocal lattice vectors (filled blue dots), and a corresponding rotation of the zone corner K points (red dots). The offset points K and $K(\theta)$ become coincident in the extended zone after translations by a particular pair of reciprocal lattice vectors.

are coincident lattice translations of each of the layers, its reciprocal space can also be indexed by a reciprocal lattice spanned by momenta with *four* integer indices describing all linear combinations of the primitive reciprocal lattice translations of each of the layers, in the manner

$$\vec{\mathcal{G}}_{p,q,p',q'} = p\vec{G}_1 + q\vec{G}_2 + p'\vec{G}_1' + q'\vec{G}_2' \tag{8}$$

This demonstrates that the primitive $\vec{G}$'s and $\vec{G}'$'s and all possible combinations $\vec{G} + \vec{G}'$ are in the reciprocal lattice of the faulted structure. The smallest nonzero combinations of these vectors have length $4\pi/\sqrt{3(m^2 + mn + n^2)}$ and span the first star of reciprocal lattice vectors of the commensuration supercell.

A critical question is whether the momentum offset $\vec{K}(\theta) - \vec{K}$ or $K(\theta) - \vec{K}'$ are *also* in the reciprocal lattice of the commensuration cell. For the former situation this is the question of whether

$$\vec{K}(\theta) - \vec{K} = \vec{\mathcal{G}}_{p,q,p',q'} = p\vec{G}_1 + q\vec{G}_2 + p'\vec{G}_1' + q'\vec{G}_2' \ (?) \tag{9}$$

for some choice of integers (p, q, p', q'). Representing these two dimensional vectors by complex numbers one finds that Eqn. 9 can be expressed

$$e^{i\theta_{mn}} = \frac{1 + \sqrt{3}\left(pe^{i\pi/6} + qe^{-i\pi/6}\right)}{1 + \sqrt{3}\left(p'e^{-i\pi/6} + q'e^{i\pi/6}\right)} \tag{10}$$

where θ_{mn} is given by Eqn. 2. Nontrivial solutions invert the indices $p' = q$ and $q' = p$ and lead to the matching condition

$$p = \frac{m - n - 3mq}{3n} \tag{11}$$

Thus $\vec{K}(\theta) - \vec{K}$ is in the reciprocal lattice only for *supercommensurate* structures where $m - n$ is a multiple of 3. Eqn. 11 is identical to Eqn. 7 that identifies the even sublattice exchange commensurations, so that sublattice "even" structures always allow intravalley interlayer coupling. For example, when $(m, n) = (2, 5)$ we have $\theta = 27.796°$ and the first integer solutions to Eqn. 10 occur for $q = 3$ for which $p = 1$ and $(p', q') = (3, 1)$.

The existence of this solution implies that these K points are coincident in the extended zone after translations by $p\vec{G}_1 + q\vec{G}_2$ and $p'\vec{G}_1' + q\vec{G}_2'$ as illustrated in the right panel of Fig. 3.

One can also ask about the possibility of commensurability for intervalley momentum transfer $K(\theta) - K'$, namely

$$\vec{K}(\theta) - \vec{K}' = \vec{\mathcal{G}}_{p,q,p',q'} = p\vec{G}_1 + q\vec{G}_2 + p'\vec{G}_1' + q'\vec{G}_2' \,(?) \tag{12}$$

Following a similar line of analysis one finds a different set of commensurability conditions

$$
\begin{aligned}
p &= \frac{m(q+1) - nq}{m + 2n} \\
p' &= \frac{nq - m(1+q)}{m + 2n} \\
q' &= \frac{(2m+n)q + m}{m + 2n}
\end{aligned}
\tag{13}
$$

Thus for example, $m = 1$, $n = 3$ gives a rotation angle $\theta = 32.204°$ which has its first integer solution when $\tilde{q} = q = 4$, giving $(p,q) = (-1,4)$ and $(p',q') = (1,3)$. Notice the asymmetry between the values of (p,q) and (p',q'): the scattering between inequivalent Dirac cones requires *different* umklapp terms when indexed to the individual reciprocal lattices of the two layers. The indices would be reversed by considering $K \to K'(\theta)$ couplings. This matching rule implies that $\vec{K}(\theta)$ and $\vec{K}'$ are coincident in after translations by $p\vec{G}_1 + q\vec{G}_2$ and $p'\vec{G}_1' + q\vec{G}_2'$ as illustrated in the left panel of Fig. 3.

One can prove that Eqns. 9 and 12 cannot be simultaneously satisfied for a common rotation angle. For example if $m = 3\mu + 1$ and $n = 3\nu + 1$ then $m - n$ is a multiple of 3 and intravalley couplings are in the reciprocal lattice. In this situation Eqn. 13 requires that

$$p = \frac{3(\mu q - \nu q + \mu) + 1}{3(\mu + 2\nu + 1)} \tag{14}$$

which is impossible since the numerator is never divisible by 3 so that intervalley coupling is excluded. On the other hand, when $m = 3\mu \pm 1$ and $\nu = 3\nu \mp 1$ intravalley are excluded and

$$p = \frac{(3(\mu - \nu)q + \mu) + 2q + 1}{3(\mu + 2\nu) \mp 1} \tag{15}$$

which can be satisfied for integer p by appropriate choice of integer q so that intervalley coupling is allowed. These two possibilities are thus complementary and mutually exclusive: one or the other must occur if the rotation is commensurate. Using the indexing rule Eqn. 4, one can easily show that partner commensurations realize complementary commensuration conditions: one member admits only the intravalley interlayer coupling while the other allows only the analogous intervalley scattering. Thus the valley structure of the interlayer couplings are specified by the sublattice exchange symmetry of the structure.
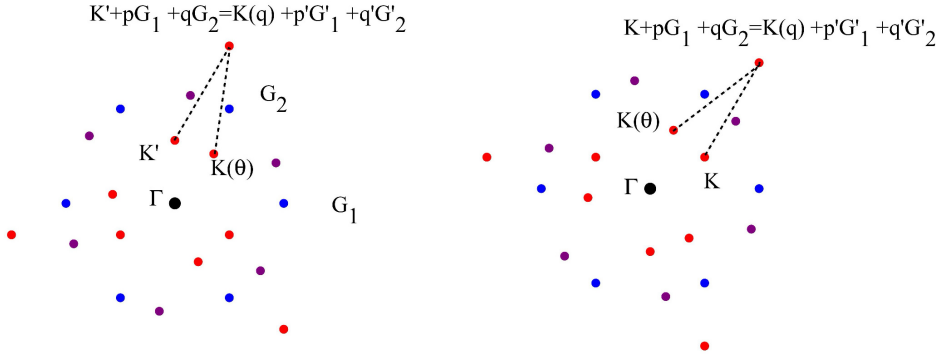
Figure 3. Commensurability conditions in reciprocal space for partner commensurations at (left) $\theta = 21.787°$ $((m,n) = 1,3)$ and (right) $\theta = 38.213°$ $((m,n) = (2,5))$. In the left panel the lattice structure is odd under sublattice exchange and the offset $K(\theta) - K'$ (red dots) is in the reciprocal lattice of the commensuration cell. Translation by particular layer reciprocal lattice vectors (spanned by the layer reciprocal lattice vectors and their rotated counterparts, shown as the blue and violet points, respectively) brings these two momenta into coincidence in the extended zone. In the right panel the lattice structure is even under sublattice exchange and the offset $K(\theta) - K$ is in the reciprocal lattice of the commensuration cell. Translation by different layer reciprocal lattice vectors brings these two momenta into coincidence in the extended zone. These two commensuration conditions are complementary and mutually exclusive.

3. Layer Decoupling by Rotational Mismatch

Early work on the electronic properties of twisted graphene bilayers recognized that small angle rotational faults are inevitably described by large period commensuration cells that make atomistic calculations impractical. Instead it is useful to develop a long wavelength description that captures the effect of rotation on the low energy electronic structure. The essential physics in this treatment is the momentum offset of the Dirac nodes produced by the rotation [17] as illustrated in Fig. 2.

The starting point of the continuum theory is the long wavelength theory appropriate to *single layer* graphene. The effective mass theory for electrons in each valley introduces two Dirac Hamiltonians for their smoothly varying pseudo-spinor fields

$$H_K = -i\hbar v_F \sigma \cdot \nabla; \; H_{K'} = \sigma_y H_K \sigma_y \tag{16}$$

where the σ's are 2×2 Pauli matrices acting on the sublattice amplitudes. A small angle relative rotation of the crystallographic axes in the of the two layers offsets the crystal momenta of their closest Dirac nodes by $\Delta K = 2K \sin(\theta/2)$. This can be described by a pair of layer-polarized Dirac Hamiltonians parameterized by the momentum offset $\Delta \vec{K} = \vec{K}(\theta) - \vec{K}$ in the manner

$$H_K \quad = \hbar v_F \sigma \cdot (-i\nabla - \frac{\Delta \vec{K}}{2})$$

$$H_{K(\theta)} = \hbar v_F \sigma^\theta \cdot (-i\nabla + \frac{\Delta \vec{K}}{2}) \tag{17}$$

where $\sigma_\mu^\theta = \exp(i\sigma_z\theta/2)\sigma_\mu \exp(-i\sigma_z\theta/2)$ because of the relative rotation of the two layers.

Electrons in neighboring layers are coupled by a θ-dependent interlayer coupling amplitude projected into the pseudospin basis. For small angle rotations these interlayer amplitudes vary smoothly in real space and one can focus on their lowest Fourier components. In the theory of Lopes dos Santos *et al.* [17] the offset momentum $\Delta \vec{K}$ is not in the reciprocal lattice of the commensuration cell and these authors focus on the three momenta $\vec{\mathcal{G}}_i$ that leave the offset $|\vec{K}(\theta) - \vec{K} - \vec{\mathcal{G}}_i|$ invariant. These momenta can be expressed in terms of the offset ΔK: in complex notation they are $\mathcal{G}_i = (0, \mathcal{G}_1 = \sqrt{3}e^{i\pi/6}\Delta K, \mathcal{G}_1 + \mathcal{G}_2 = \sqrt{3}e^{-i\pi/6}\Delta K)$. In the pseudospin basis, the interlayer coupling for each of these momentum transfers is characterized by a 2×2 matrix-valued tunneling coefficient $T(\mathcal{G})$ whose elements have been estimated numerically using a tight binding model. This yields in the small angle limit

$$T(\mathcal{G} = 0) = \tilde{t}_\perp \begin{pmatrix} 1 & 1 \\ 1 & 1 \end{pmatrix}; \quad T(\mathcal{G} = -\mathcal{G}_1) = \tilde{t}_\perp \begin{pmatrix} z & 1 \\ \bar{z} & z \end{pmatrix}$$

$$T(\mathcal{G} = -(\mathcal{G}_1 + \mathcal{G}_2)) = \tilde{t}_\perp \begin{pmatrix} \bar{z} & 1 \\ z & \bar{z} \end{pmatrix} \tag{18}$$

where $z = e^{2\pi i/3}$, $\bar{z} = e^{-2\pi i/3}$ and $\tilde{t}_\perp \sim 0.11\,\mathrm{eV}$, approximately independent of the supercell period.

The asymmetry in the set of selected $\vec{\mathcal{G}}$'s appearing in Eqn. 18 occurs because of the choice of the reference valley for the long wavelength expansion. Nevertheless, this approach explicitly preserves the threefold rotational symmetry of the commensuration cell. This is seen most clearly by observing that the T matrices are off diagonal operators in the layer degree of freedom and one may therefore arbitrarily "shift" the interlayer coupling momenta by a layer-dependent $U(1)$ gauge transformation. In particular the gauge shift $e^{-i\Delta \vec{K} \cdot \vec{r}}$ in the rotated layer brings the two Dirac nodes into coincidence and shifts the three momentum transfers so that they form the three arms of a star generated by $Q = -\Delta K$ and its $\pm 2\pi/3$-rotated partners. The negates of these three momenta occur in the reciprocal amplitudes describing the reverse tunneling processes. Thus the expansion about a *single* zone corner point preserves the full three fold symmetry of the commensuration cell, as required

The essential features of this theory are (1) the existence of a crystal momentum offset due to the rotational fault, (2) the coupling of plane wave states in one layer to a triad of plane wave states in its neighbor and (3) the existence of a $\mathcal{G} = 0$ term in the effective interlayer tunneling Hamiltonian. Feature (1) suggests that at sufficiently low energy the effect of the interlayer coupling can be treated perturbatively in the dimensionless coupling parameter $\Gamma = \tilde{t}_\perp/\hbar v_F \Delta K$. Feature (2) implies the perturbative effects of this coupling *vanish by symmetry* precisely at $E = 0$ so that the coupled system preserves the Dirac nodes of its two (decoupled) layers. Perturbative effects of

the coupling arise at linear order in the momentum differences $\vec{k} \pm \Delta\vec{K}/2$ and can be interpreted as a twist dependent renormalization of the Fermi velocity

$$\frac{v_F^*}{v_F} = 1 - 9\left(\frac{\tilde{t}_\perp}{\hbar v_F \Delta K}\right)^2 \tag{19}$$

Equation 19 needs to be applied with care since it breaks down both in the limit of small rotation angles due to a failure of the perturbation theory when $\Delta K \to 0$ and at large rotation angles when commensuration effects, neglected in this treatment, can intervene. Finally, feature (3) indicates that electron states in the two layers that have the *same* crystal momentum modulo $\vec{\mathcal{G}}$ are coupled through the interlayer Hamiltonian. In the low energy theory the layer-polarized Dirac cones degenerate in the planes that bisect lines connecting their nodes (above the crossover energy $\hbar v_F \Delta K/2$) and one expects the strongest interlayer mixing to occur in these planes. There are three such planes that bisect the lines along ΔK and its $\pm 2\pi/3$ rotated counterparts. The onset of this mixing is associated with a change of topology of the bilayer bands, connecting a low energy sector with layer-decoupled Dirac cones to higher energy layer-coherent hyperbolic bands. In the lowest band this transition is associated with a saddle point in the electronic spectrum and a logarithmic van Hove singularity in the two dimensional density of states [18].

4. Atomistic Calculations

The novel physics of rotationally-induced layer decoupling has stimulated theoretical work by several groups to explore this effect using various atomistic models. Ab initio calculations have been carried out for misaligned bilayer supercells containing up to ~ 500 atoms ($\theta \sim 5°$) while tight binding methods have allowed workers to access larger systems of up to 15000 atoms [10, 21, 22, 23, 24]. These studies have examined the Fermi velocity renormalization, the form of the low energy electronic spectrum near the K points and the spatial modulation of the electronic charge density.

Much of the ab-initio work has understandably focused on the shortest period twisted structures, e.g. $\sqrt{7} \times \sqrt{7}$ and $\sqrt{13} \times \sqrt{13}$ commensurations [10, 23]. Calculations on these systems generally confirm a suppression of the interlayer coupling scale and a Fermi velocity near the K point which is essentially indistinguishable from that of single layer graphene. The most thorough investigation of the Fermi velocity renormalization has been given by de Laissardière *et al.* [22] who suggest that the rotational faults are characterized by three different velocity renormalization regimes, determined by the fault angle: (a) $15° < \theta < 30°$ where the Fermi velocity is essentially the same as for single layer graphene, (b) $3° < \theta < 15°$ where a downward renormalization is found, well described by the perturbation theory of [17], and a low angle regime $\theta < 3°$ where the low energy bands are flattened and not described by the perturbative treatment. The small renormalization in the large fault angle regime (a) is at least qualitatively consistent with the continuum theory since the renormalization occurs via a virtual mixing of low energy states with states separated by an energy barrier $\hbar v_F \Delta K$. The

breakdown of the perturbation theory for sufficiently small angle faults is similarly understandable since it involves an expansion in $\tilde{t}_{\perp}/\hbar v_F \Delta K$. Surprisingly, in this low angle regime de Laissardière *et al.* also report a pronounced spatial modulation of the low energy eigenstates that tends to localize their charge densities in spatial regions locally characterized by "AA" stacking, suggesting some form of multiband physics that is not captured by the truncated continuum model. The accuracy of the perturbation theory in the intermediate regime has been further questioned by the density functional calculations of Shallcross *et al.* [23] who find that the bilayer v_F is nearly equal to that of single layer graphene down to smallest angles ($\sim 9°$) they were able to study.

The calculations by Shallcross *et al.* [23] also reveal features in the electronic spectra near the K points that are not captured by the primitive continuum theory. Significantly, close to the zone corners the electronic bands are *not* linear but instead they are mixed, which requires an interlayer mass operator in the low energy Hamiltonian. Interestingly the spectral structure, and therefore the matrix structure of this mass term, is *different* for partner commensurations and therefore it cannot be determined solely by the size of the commensuration cell. The scale of the mixing is nevertheless small relative to its value for Bernal bilayers, e.g. the mixing scale for the $\theta = 30° \pm 8.213°$ structure is $\approx 7\,\mathrm{meV}$ compared to $\approx 0.2\,\mathrm{eV}$ for Bernal stacking [3, 4, 26]. Further, over the range of structures they studied this mass scale appears to a rapidly decreasing function of the commensuration cell period. But the existence of this mass matrix in the low energy theory presents a significant challenge to the interpretation of the electronic states even at energies *above* the mass scale. Notably, in order to match smoothly to these low energy eigenstates the bilayer eigenstates at higher energy must be (nearly) *equal weight* states coherently mixed between the two layers instead of the layer-polarized eigenstates that one would infer from the momentum space structure of the continuum theory .

5. Second Generation Continuum Theories

There has been progress in the development of new long wavelength models that extend the physics identified in the original continuum formulation [17]. These theories examine the effects of lattice commensuration [19] and of multi-band mixing [25] on the low energy electronic structure. The former turn out to be most important for large angle faults while the latter are critical to the physics at small rotation angles. The new models are also formulated as continuum theories in order to circumvent the technical difficulty posed by fully microscopic atomistic treatments of large commensuration cells. Concurrently there has been an effort to distill the original continuum model to a simpler effective two band model [27, 28] in an effort to explore the effects of the novel band topology on the orbital quantization of its electronic states in a perpendicular magnetic field. We refer to all these new models as "second generation" continuum theories.

5.1. Interlayer Matrix Elements

A microscopic theory of the interlayer coupling can be formulated in the basis of Bloch orbitals

$$\psi_\alpha(\vec{k}) = \frac{1}{\sqrt{N}} \sum_{\vec{T}} e^{i\vec{k}\cdot(\vec{T}+\vec{\tau}_\alpha)} \phi_\alpha(\vec{T}) \tag{20}$$

where $\phi_{\alpha=(A,B)}$ are orbitals centered at positions $\vec{T} + \vec{\tau}_\alpha$ and $\vec{T}$ is a lattice translation. In this basis the interlayer Hamiltonian is

$$\langle \psi_\beta(\vec{k'})|\mathcal{H}|\psi_\alpha(\vec{k})\rangle = \frac{1}{N} \sum_{\vec{T},\vec{T'}} e^{-i\vec{k}\cdot(\vec{T'}+\vec{\tau}_\beta)} \langle \phi_\beta(\vec{T'})|\mathcal{H}|\phi_\alpha(\vec{T})\rangle e^{i\vec{k}\cdot(\vec{T}+\vec{\tau}_\alpha)} \tag{21}$$

Assuming that the inter-site tunneling amplitude depends on the layer-projected difference coordinate, the matrix element can be expressed

$$\langle \phi_\beta(\vec{T'})|\mathcal{H}|\phi_\alpha(\vec{T})\rangle = \frac{1}{(2\pi)^2} \int d^2q\, f(\vec{q})\, e^{i\vec{q}\cdot(\vec{T'}+\vec{\tau}_\beta'-\vec{T}-\vec{\tau}_\alpha)} \tag{22}$$

Carrying out the lattice sums in Eqn. 21 and expressing the momenta in terms of their differences from the respective zone corners, $\vec{k} = \vec{K} + \vec{q}$, one obtains an expression for the interlayer tunneling amplitude in terms of sums over the reciprocal lattices of the reference ($\vec{G}$) and rotated ($\vec{G'}$) layers

$$\mathcal{T}_{\beta\alpha}(\vec{q'},\vec{q}) = \frac{1}{\mathcal{A}} \sum_{\vec{G},\vec{G'}} f(\vec{q}+\vec{K}+\vec{G})\, e^{i\vec{G'}\cdot\vec{\tau}_\beta} e^{-i\vec{G}\cdot\tau_\alpha}$$

$$\delta(\vec{q'} - \vec{q} + \Delta K + \vec{G'} - \vec{G}) \tag{23}$$

where $\mathcal{A}$ is the area of the unit cell.

When $q \ll G$ Eqn. 23 describes two distinct types of interlayer tunneling processes: (1) Direct interlayer terms conserve the *crystal momentum* $\vec{k}$ and occur when $\Delta K = |\vec{K}(\theta) - \vec{K} + \vec{G'} - \vec{G}|$. (Note that this occurs for $\vec{G} = \vec{G'} = 0$ and for all boosts by the reciprocal lattice vectors $\vec{\mathcal{G}} = \vec{G'} - \vec{G}$ that symmetrically shift the initial and final states to nearby valleys.) (2) Indirect interlayer terms conserve the *Dirac momentum* $\vec{q}$ and occur when $\vec{K} + \vec{G} = \vec{K}(\theta) + \vec{G}$. The matrix element for this latter process is dominated by the Fourier amplitude of the tunnelling potential at the first momentum $\vec{K} + \vec{G}_c$ in the extended zone where the zone corner points coincide. Processes (1) and (2) have very different character. In the Dirac language, process (1) requires $\vec{q} \neq \vec{q'}$ and provides a microscopic basis for the continuum formulation of Lopes dos Santos *et al.* [17]. By contrast process (2) allows (indeed requires) $\vec{q} = \vec{q'}$ coupling and in particular it provides a mechanism for *coupling between the tips of the Dirac cones in neighboring layers*. It can be understood as an interlayer umklapp process whereby the scattering by a reciprocal lattice vector of the commensuration cell provides precisely the right momentum to bridge the momentum offset ΔK. The ratio of the amplitudes for the indirect and direct couplings is approximately $f(|\vec{K} + \vec{G}|)/f(|\vec{K}|)$ so that the indirect term is generally weaker than the direct term.

5.2. Superlattice Commensuration Effects

As discussed in Section 2.2 either $K \to K(\theta)$ or $K' \to K(\theta)$ couplings are in the reciprocal lattice of the commensuration cell for a faulted bilayer, depending on the sublattice symmetry, and using Eqn. 23 they are allowed interlayer tunnelling processes. The low energy theory is fundamentally changed by these terms since they introduce an interlayer mass operator in the long wavelength Hamiltonian. Interestingly, the analytic structure of this mass matrix is determined solely by the sublattice symmetry of the commensuration. Thus one can define two complementary families of commensurate faults where all members of a common family have a common form for their low energy Hamiltonians. The energy scale of this mass operator depends on the period of the commensuration, and it is largest for low order commensurate rotations. The primitive stacked structures with AB and AA stacking are parent structures for this family behavior which give prototypical examples for the interlayer mixing possible for generic commensurate bilayers.

The commensuration physics for these systems can be understood most easily by explicitly writing the layer Bloch states in real space in the "first star" approximation that retains only the three reciprocal lattice vectors that keep the combination $\vec{K} + \vec{G}$ to the first star of K points

$$\Psi(\vec{r}) = \sum_{\alpha} \Phi_{\alpha}(\vec{r}) u_{\alpha}(\vec{r}); \Phi_{\alpha}(\vec{r}) = \frac{1}{\sqrt{3}} \sum_{m=1}^{3} e^{i\vec{K}_m \cdot (\vec{r} - \vec{\tau}_{\alpha})} \tag{24}$$

The coupling between layers is a functional of the Bloch fields $\Psi(\vec{r})$ and its properties are captured by the local functional

$$U = \frac{1}{2} \int d^2 r \, T_{\ell}(\vec{r}) |\Psi_1(\vec{r}) - \Psi_2(\vec{r})|^2 \tag{25}$$

where T_{ℓ} is a real modulated supercell-periodic function arising from the lattice structure of the commensuration cell. The coupling function acts to correlate the amplitudes and phases of the Ψ's in the neighboring layers. The purely *local* coupling between layers in Eqn. 25 can be readily generalized to describe interlayer coupling with a finite range without substantially changing the physics. Equation 25 describes a coupled mode theory where the full Bloch waves Ψ of the two layers (importantly these are *not* the Dirac envelope functions $u_{\alpha}(\vec{r})$) are coupled by through a local spatially modulated potential.

Although the exact form of the coupling function $\mathcal{T}_{\ell}$ is unknown its important properties are constrained by symmetry: it is a real supercell-periodic function with local maximum near aligned sites of the two layers and with minima for regions where atoms in neighboring layers are out of registry. A useful analytic model satisfying these constraints can be constructed from the elementary density waves in each of the layers

$$n_{\mu=1,2}(\vec{r}) = \sum_{m \in [1]} \sum_{\alpha = A,B} e^{i\vec{G}_{\mu,m} \cdot (\vec{r} - \vec{\tau}_{\mu,\alpha})} \tag{26}$$

summed over the first star of reciprocal lattice vectors in the μ-th layer. Then, a

nonlinear functional of the density fields that satisfies all the symmetry constraints is

$$T_\ell(\vec{r}) = C_0 e^{C_1(n_1(\vec{r}) + n_2(\vec{r}))} \tag{27}$$

The sum of the layer density waves is a real function with the translational symmetry of the commensuration cell and no shorter. Eqn. 27 is maximized at special positions where the two density functions in each layer are separately maximized corresponding to aligned atomic sites, and it exhibits exponential suppression in regions where the density waves are out of registry. This ansatz for the coupling function has some important features. (1) It is a nonlinear function of the primitive reciprocal lattices vectors of each of the layers so that *all* the reciprocal lattice vectors of the commensuration cell are are represented in an expansion of the exponential in powers of its argument. (2) It is a separable function, constructed from a product of functions each of which is spanned by the *separate* reciprocal lattices of the two layers. (3) It is parameterized by two constants C_0 and C_1 which respectively describe the strength and range of the microscopic interlayer tunneling amplitudes. (Thus for example, very long range hopping is described by a small value of C_1.) The two constants C_0 and C_1 can be estimated from microscopic theory.

Figure 4 gives a density plot of the local coupling function $T_\ell(\vec{r})$ calculated for partner commensurations at $\theta = 21.787°$ and $\theta = 38.213°$. The former corresponds to a sublattice exchange "odd" structure and has a threefold rotational symmetry. Its partner is a sublattice exchange "even" structure and retains the full sixfold symmetry of the graphene layer, though on an inflated commensuration supercell. This illustrates a general property of all "odd" and "even" commensurate faults. The patterns shown in this density plot provide a real space image of the interlayer resonance pattern for a twisted bilayer. Interestingly, for large angle faults, one finds that the appearance of *fivefold* resonance rings (due to rotated misaligned hexagons) is a robust motif in the coupling function. For small angle faults the coupling function is described instead by the familiar Moire pattern that evolves smoothly between zones locally defined by by AB, BA and AA stacking.

The couplings between the Dirac fields u_α in neighboring layers are obtained from the cross terms in Eqn. 25 after integrating out the lattice scale oscillations and are given by the Fourier transform of T_ℓ on the reciprocal lattice of the commensuration cell $t(\vec{\mathcal{G}})$. The $\vec{\mathcal{G}} = 0$ term describes the crystal momentum-conserving interlayer couplings discussed in the theory of Lopes dos Santos *et al.* [17]. In addition there are umklapp terms involving $\vec{\mathcal{G}} \neq 0$ terms that express the symmetry allowed couplings between Dirac nodes $K_m \rightarrow K_{m'}(\theta)$. The geometrical considerations of Section 2.2 require that for any given commensuration there are couplings within two distinct pairs of Dirac nodes at the corners of their respective Brillouin zones. In the Bloch basis these matrix elements are spanned by a 3×3 matrix of finite momentum scattering amplitudes $\hat{V}_{\mathrm{ps}}$ which,
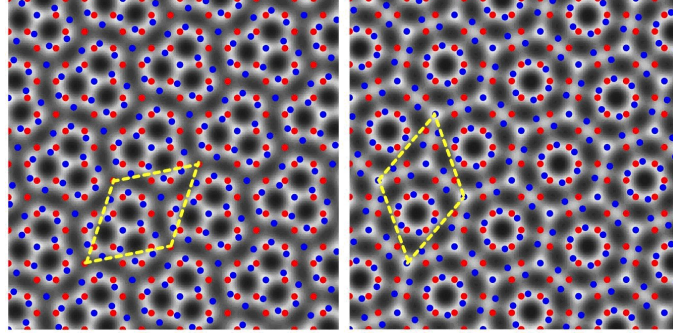
Figure 4. The spatial dependence of the interlayer coupling function $T_\ell(\vec{r})$ of Eqn. 27 is illustrated by these greyscale plots for commensurate faults at $21.787°$ (left) and $38.213°$ (right). The left structure has odd sublattice exchange parity, the right structure is even. The left pattern has a threefold rotational symmetry, the right pattern has the sixfold symmetry of an isolated graphene sheets. Both patterns contain combinations of fivefold resonance rings that are combined in clusters to form a periodic two dimensional pattern. Adapted from reference [19].

using the threefold rotational symmetry, takes the form

$$\hat{V}_{\text{ps}} = \begin{pmatrix} V_0 & V_1 & V_2 \\ V_2 & V_0 & V_1 \\ V_1 & V_2 & V_0 \end{pmatrix} \tag{28}$$

Here V_0 describes the scattering amplitude for a momentum transfer $\mathcal{G} = |\Delta\vec{K}|$ coupling the two layers while V_1 and V_2 describe scattering amplitudes with larger momentum transfers $\sim \vec{G}$. By projecting Eqn. 28 onto the sublattice (pseudospin) basis, one obtains the 2×2 interlayer mass matrices $\hat{\mathcal{H}}_{\text{int}}$ that couple the Dirac fermions of the two layers. The low energy Hamiltonian for an even bilayer is thus expressed as a 4×4 matrix (acting on the two sublattice and two layer degrees of freedom)

$$\hat{\mathcal{H}}_{\text{even}} = \begin{pmatrix} -i\hbar\tilde{v}_F\sigma_1\cdot\nabla & \hat{\mathcal{H}}_{\text{int}}^+ \\ (\hat{\mathcal{H}}_{\text{int}}^+)^\dagger & -i\hbar\tilde{v}_F\sigma_2\cdot\nabla \end{pmatrix} \tag{29}$$

while for the odd bilayer

$$\hat{\mathcal{H}}_{\text{odd}} = \begin{pmatrix} -i\hbar\tilde{v}_F\sigma_1\cdot\nabla & \hat{\mathcal{H}}_{\text{int}}^- \\ (\hat{\mathcal{H}}_{\text{int}}^-)^\dagger & i\hbar\tilde{v}_F\sigma_2^*\cdot\nabla \end{pmatrix} \tag{30}$$

where σ_n are Pauli matrices acting in the sublattice pseudospin basis of the $n-th$ layer and $\tilde{v}_F$ is the renormalized Fermi velocity. Note that for even parity faults the bilayer Hamiltonian couples nodes of the same chirality, whereas the odd parity faults introduce coupling between nodes of compensating chirality. In either case the spectrum for coupled system retains a two-valley character due to the two ways of matching nodes in either family of structures. The interlayer mass matrices $\hat{\mathcal{H}}_{\text{int}}^\pm$ are

$$\hat{\mathcal{H}}_{\text{int}}^+ = \mathcal{V}e^{i\vartheta}\begin{pmatrix} e^{i\varphi/2} & 0 \\ 0 & e^{-i\varphi/2} \end{pmatrix}, \quad \hat{\mathcal{H}}_{\text{int}}^- = \mathcal{V}e^{i\vartheta}\begin{pmatrix} 1 & 0 \\ 0 & 0 \end{pmatrix} \tag{31}$$

Eqns. 29 and 31 show that for sublattice "even" faults the mass term involves an xy rotation of its pseudospin through angle φ. This angle can not be identified with the rotation angle θ but it results instead from the interference of the three complex scattering amplitudes V_i. By contrast in Eqns. 30 and 31 one finds that interlayer motion across an "odd" fault is mediated by the amplitude on its dominant eclipsed sublattice. In both mass matrices the overall phase of the operator ϑ can be removed by a gauge transformation.

Eqn. 31 describes a coupling between Dirac waves in the neighboring layers that persists in the long wavelength $q \to 0$ limit, qualitatively changing the structure of the low energy spectra. Their effects are illustrated in Figure 5. For sublattice odd parity faults one pair of coupled bands are gapped on the interaction scale $\mathcal{V}$ leaving an $E = 0$ contact point between a second pair of quadratically dispersing bands. For the even parity structures the $q = 0$ spectrum contains a pair of coherence-split doublets. These two doublets are the symmetric and antisymmetric combinations of the original single layer Dirac modes; interestingly the layer-coupled states are topologically required to retain their Dirac character for small q, and disperse linearly away from the points of degeneracy. At finite momentum two branches undergo an avoided crossing which gaps the spectrum at its charge neutrality points. Thus these structures are generically *fully gapped* where the size of the gap is determined by the pseudospin rotation angle φ in Eqn. 31 which allows these branches to hybridize. This gap degenerates to zero for the special case of an AA stacked structure where $\varphi = 0$ by symmetry. In both cases the residual effect of the mixing at high energy is to introduce a coherence splitting between two linearly dispersing layer-hybridized bands.

Both these behaviors have precise analogs for the limiting cases of Bernal and AA stacked bilayers which can be understood as the primitive parent structures of these two families. As shown in the lower left panel of Fig. 5 the Bernal spectra exhibit the mass structure expected for all sublattice exchange odd faults, though on an inflated energy scale ($\approx 0.2\,\text{eV}$) reflecting the full alignment of all sites on a single sublattice. Similarly the primitive AA stacking features a coherence splitting of its bonding and antibonding layer-coupled states, but without the pseudospin rotation φ so that the spectrum remains gapless and the zero energy states occur on a ring in reciprocal space.

5.3. Nonlocal Potential Scattering

For small rotation angle the offset momentum $\Delta K \to 0$ and perturbation theory in the dimensionless parameter $\tilde{t}_\perp / \hbar v_F \Delta K$ fails. The breakdown of the perturbation theory occurs because of an incomplete treatment of multiple scattering processes involving the interlayer coupling operator. Recognizing this, Bistritzer and MacDonald (BM) [25] developed a theory that treats multiple scattering through the three fundamental interlayer amplitudes that describe a spatially modulated interlayer coupling with the period of the commensuration supercell. Their results show that the Fermi velocity renormalization of the perturbation theory presages more dramatic physics at small
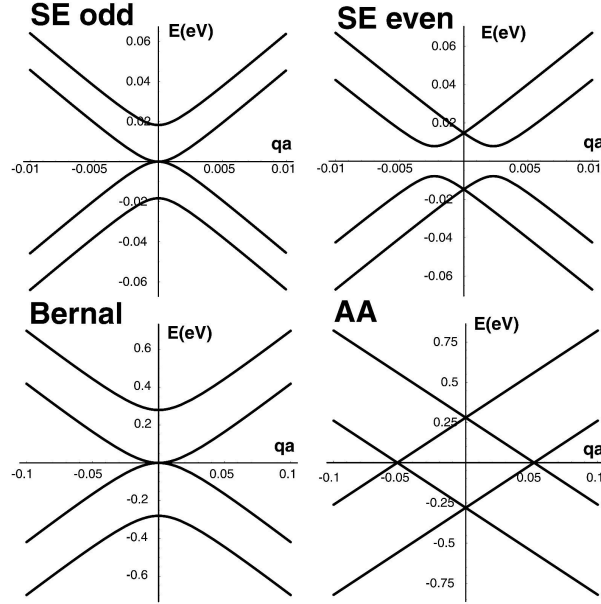
Figure 5. The low energe electronic structure for the sublattice exchange odd parity $\theta = 21.787°$ commensuration and the partner even parity $38.213°$ structure are compared with the spectra for the parent Bernal (AB) and AA stacked structures. All odd parity structures, as shown on the left, contain a pair of coherence split massive bands and a contact point between two quadratic bands at $E = 0$. The even parity structures, shown on the right, feature a bonding/antibonding splitting, with a fully developed gap near the charge neutrality point which degenerates to a gapless state for the AA stacked structure. Adapted from reference [19].

rotation angle which can be described as "velocity reversal," i.e. the Fermi velocity changes *sign* as a function of (small) rotation angle crossing through zero at a series of discrete magic angles. As a consequence the small angle regime is predicted to feature a manifold of nearly flat bands at low energy.

The BM model is formulated as a two layer scattering theory: states with momentum $\vec{k}$ in one layer are scattered into states at momentum $\vec{k} + \vec{Q}$ in its neighbor. In the pseudospin basis the amplitudes for these processes are the 2×2 matrices given in Eqn. 18. The gauge transformation $e^{-i\Delta\vec{K}\cdot\vec{r}}$ on the rotated layer brings two Dirac nodes of neighboring layers into coincidence, and in this momentum shifted basis the three momentum transfers $\vec{Q}_{i(=0,\pm1)}$ are $Q_0 = -\Delta\vec{K}$ and two $\pm 2\pi/3$-rotated partners $Q_{\pm1}$ which form a threefold symmetric triad. Thus this construction considers a twofold layer-degenerate Dirac cone whose states are coupled through an off-diagonal nonlocal operator containing three possible momentum transfers $\vec{Q}_i$ in the interlayer hopping. In the long distance theory the single layer Hamiltonians are isotropic, so for *arbitrary* rotation angle θ the the theory is specified by its unrenormalized Fermi velocity, the rotation angle and the coupling strength labelled w in BM [25], which combine to form a single dimensionless scaling parameter $\alpha = w/2\hbar v_F \sin(\theta/2)$.
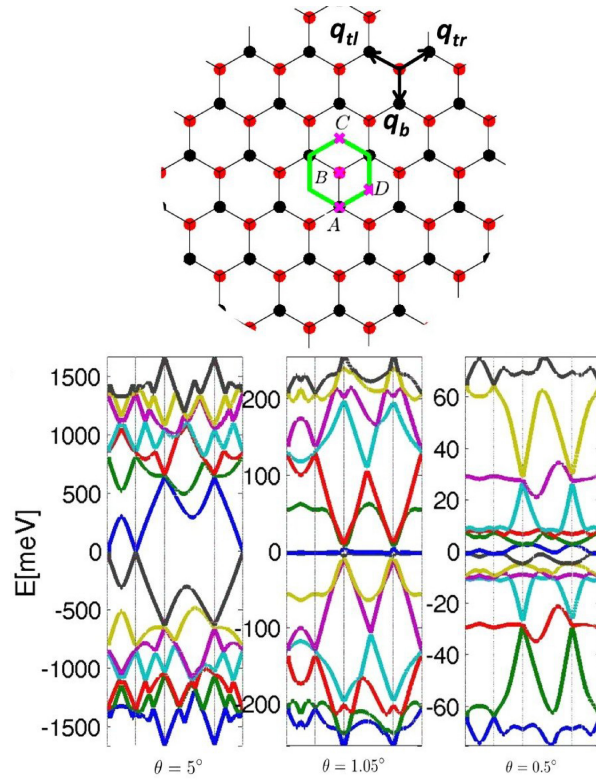
Repeated action of the nonlocal interlayer operator generates a lattice of coupled

momenta as shown in the top panel of Figure 6. The interlayer tunneling amplitudes are *directed transitions* in reciprocal space: the momenta Q_i and their negates $-Q_i$ describe complementary processes that transport electrons to and from the rotated layer. Consequently, an even number of applications of the nonlocal operator to an initial single-layer Bloch state at wavevector $\vec{k}$ generates a Bloch state in the same layer with momentum $\vec{k} + \vec{\mathcal{Q}}$ where $\vec{\mathcal{Q}}$ is spanned by the primitive vectors $\vec{Q}_1 - \vec{Q}_0$ and $\vec{Q}_{-1} - \vec{Q}_0$. This defines a triangular reciprocal lattice whose six first star elements have magnitude $\sqrt{3}\,Q_0$, and are 90° rotated with respect to the original $\pm\vec{Q}_i$'s. An odd number of applications of the operator transports the electron to the neighboring layer on the same reciprocal lattice, but offset by the momentum shift $\vec{Q}_0$. The combination of these two sets describes a honeycomb lattice where the alternating sites (momenta) occupy different layers as shown in Fig. 6.

BM studied this model by numerically diagonalizing a truncated Hamiltonian expanded in a plane wave basis and retaining plane waves with kinetic energies below the coherence scale $\sim w$. The effects of multiple scattering through the interlayer coupling terms is then encoded in the structure of the bilayer eigenstates which contain coherent superpositions of the single-layer Dirac modes. For large rotation angles ($\theta > 3°$) the model reproduces the perturbation theory of Lopes dos Santos et al. By contrast, in the very small angle regime the bandwidth $\hbar v_F Q_0$ collapses, the number of elements in the low energy basis grows correspondingly and the electronic structure becomes spectrally congested as illustrated in Fig. 6. Thus the small angle regime is described by a strong coupled *multiband* theory that introduces physics inaccessible to a low order perturbation theory. BM find that the low energy spectra in this regime show a very substantial reduction of the Fermi velocity (typically < 0.1 of its single layer value) due to level repulsion among the coupled bands. Remarkably, the reduced velocity parameter *oscillates* as a function of the fault angle as shown in Figure 7 and crosses zero at a series of magic rotation angles. They suggest that this oscillation likely results from a θ dependence of the superpositions of single layer modes that contain velocities of opposite sign, though a complete theory of the velocity oscillations has yet to be developed. Thus the velocity renormalization found in the weak coupling limit represents just the first step towards a complete twist-induced reconstruction of the low energy spectrum!

5.4. Two Band Models

There has been interest in distilling the continuum theory to a simpler effective *two band* model that captures the topological structure of its low energy spectrum. The approach is similar in spirit to the theory of Bernal stacked bilayers [3, 26, 29] where one can integrate out its high energy degree of freedom to arrive at an effective theory for its low energy states. For the Bernal bilayer this procedure identifies a new class of layer-coherent chiral fermions that have quadratic low energy dispersion and a Berry's phase of 2π. For the twisted bilayer, neglecting commensuration effects, the low energy spectrum contains two layer-polarized *linear* Dirac cones that are recoupled at an energy

Figure 6. Top panel: A lattice of momenta is generated by repeated action of a nonlocal interlayer coupling operator on a Bloch state in a single layer. The nonlocal operator transports an electron between layers and boosts the momentum by a threefold symmetric triad of momentum transfers Q_i. An even number of applications of the operator generates a triangular lattice of momenta in the original layer (red), an odd number generates a triangular lattice offset by momentum ΔK (black). The combination forms a honeycomb lattice of coupled momenta. Bottom panel: Band structures obtained by numerical diagonalization of the continuum Hamiltonian in a truncated plane wave basis retaining kinetic energies of order the coupling strength w. The bands are plotted along the momentum space trajectory $ABCDA$ in the top figure. For small rotation angles the bands flatten and the Fermi velocity of the zero energy states is strongly suppressed. Adapted from reference [25].

scale $\hbar v_F |\Delta \vec{K}|/2$ where they merge. The two band model attempts to provide a compact description of the topological transition of the band dispersion that connects the low energy "doubled cone" sector to its high energy layer-hybridized sector.

For twisted bilayers the two band construction can be understood as a variant of the low energy theory for a Bernal bilayer that allows for a finite momentum offset $|\Delta \vec{K}|$ between its Dirac nodes. Thus the low energy theory for Bernal stacking is modified in the manner

$$\mathcal{H}_K = -\frac{\hbar^2}{m} \begin{pmatrix} 0 & \partial^2 \\ \bar{\partial}^2 & 0 \end{pmatrix} \rightarrow -\frac{\hbar^2}{m(\theta)} \begin{pmatrix} 0 & \partial^2 - (\Delta K)^2 \\ \bar{\partial}^2 - (\Delta \bar{K})^2 & 0 \end{pmatrix} \quad (32)$$

valid for very small fault angles where $\hbar v_F |\Delta K| \ll \tilde{t}_\perp$ and $m = \tilde{t}_\perp / v_F^2$. This expression
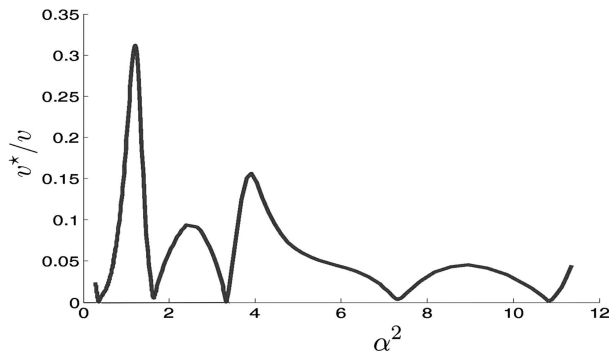
Figure 7. The magnitude of the renormalized Fermi velocity for the zero energy states is plotted as a function of the coupling parameter $\alpha^2 = (w/2\hbar v_F \sin(\theta/2))^2$ for small rotation angles. The oscillations results from sign changes of the Fermi velocity in the small rotation angle regime. For large rotation angles the renormalization factor $v^*/v \approx 1 - 9\alpha^2 \rightarrow 1$. Adapted from [25].

can be derived by replacing the interlayer operators of Eqn. 18 by a simpler expression $\tilde{t}_\perp \sigma_-$ which physically describes an interlayer tunneling amplitude across a single sublattice in each layer. The spectrum of this Hamiltonian features a pair of Dirac cones, split by the momentum offset $|\Delta \vec{K}|$, that merge at a two dimensional saddle point at $q = 0$ representing the topological transition of the band structure. Importantly, the single layer Dirac cones in this model have the *same* chirality so that annihilation of the Dirac points when they are coupled is topologically forbidden. Generically, this model does allow for an energy offset between the Dirac points of the coupled bilayer but this is believed to be small for physically reasonable coupling strengths.

The Hamiltonian in Eqn. 32 has been used to study the orbital quantization of a twisted bilayer in the presence of a perpendicular magnetic field. By construction the limit $\Delta K = 0$ describes the Landau quantization of Bernal bilayer graphene: a Berry's phase of 2π and quantized energy levels $\propto \sqrt{n(n-1)B}$. By contrast for finite rotation angles the low energy spectrum of the offset model is a "doubled" theory of single layer graphene: the fourfold degeneracy due to the spin and valley degrees of freedom is doubled by an approximate layer decoupling of its low energy eigenstates. An asymptotic analysis of the eigenvalues within this model demonstrates that splittings of the Landau level degeneracies due to interlayer coupling are exponentially suppressed as a function of the rotation angle in the low energy regime [28]. The spectrum thus features a zero mode and Landau levels that disperse $\propto \sqrt{nB}$ [27, 28]. This twofold layer degeneracy is quickly eliminated as one passes through the crossover energy $\hbar v_F \Delta K/2$ where the Dirac cones merge and hybridize. Above this crossover the spectrum has a different character: layer degeneracies are removed and the quantized energies are $\propto (n + 1/2)B$ as expected for a parabolic interlayer coherent band.

6. Discussion

Rotational faults commonly occur in a several different forms of graphene and their electronic properties are actively studied experimentally. The rapidly growing experimental literature on this subject has not yet provided a unified picture of the effects of faults on the electronic behavior, possibly due to differences in the electronic properties of samples produced by different experimental methods.

A significant point of *agreement* among the various experimental works is that the interlayer coherence scale is very small in these systems [9, 10, 14, 15]. This can be deduced clearly from their Landau level spectra which have been measured by scanning tunneling spectroscopy (STS). These spectra show a scaling of the Landau level energies $E_n \propto \sqrt{nB}$ [14, 15] the signature of the Landau quantization of a massless Dirac band, as observed for single layer graphene and quite distinct from the level sequence observed for Bernal stacked bilayers [3]. Perhaps the strongest evidence for a reduction of the interlayer coupling scale comes from angle resolved photoemission experiments which directly measure the quasiparticle dispersion relation [16, 30] and find spectra that follow the expected form for an isolated Dirac cone. These measurements have been interpreted as providing the first direct measurement of the Dirac dispersion relation in graphene, uncontaminated by substrate or other interlayer effects [16].

Since the effects of the interlayer coupling in twisted multilayers are intrinsically weak, their study is posing a significant experimental challenge. It is here where different experiments carried out on different samples disagree. For example, the Fermi velocity can be deduced from the slope of the $\sqrt{nB}$ scaling relation for the Landau quantized energies. The strongest evidence for a twist-induced renormalization of v_F comes from the Landau level spectra measured by scanning tunneling spectroscopy of CVD graphenes grown on Ni substrates [20]. This work reports that v_F is not constant as a function of scanned position across a macroscopic sample, but instead it is found to vary in a range $0.87 \times 10^6 \, \text{m/s} < v_F < 1.1 \times 10^6 \, \text{m/s}$. Simultaneous measurement of the topography of the Moire superlattice period of these samples correlates the velocity reduction with the period and hence the rotation angle. The larger value, found for large angle rotations, agrees well with the v_F for single layer graphene and the 20% reduced value is correlated with a small angle rotation $\sim 3°$ as suggested by a perturbative analysis of the continuum theory [17, 25]. This contrasts with analogous STS measurements carried out for multilayer graphenes grown epitaxially on SiC $(000\bar{1})$. These also show the $\sqrt{nB}$ scaling of the Landau quantized energies. However, for these materials the slope of the scaling relation yields a Fermi velocity $1.1 \times 10^6 \, \text{m/s}$ for all samples studied down to a rotation angle of $1.4°$ [15] completely spanning the range of rotation angles where a velocity renormalization is expected.

A similar discrepancy arises in the spectroscopy of the van Hove singularity presumed to occur in the region where the momentum-offset Dirac cones of a twisted bilayer merge. Low energy STS on Ni/CVD grown graphene reveals low energy peaks whose energies disperse with their topographically measured rotation angles in the

low angle regime $1.2 < \theta < 3.5°$ [18] roughly consistent with the van Hove scenario. Yet these features are not seen at all in spectroscopy of the SiC epitaxial twisted graphenes regardless of the fault angle. Perhaps the strongest challenge to the idea of a twist-induced spectral reconstruction comes from angle resolved photoemission. These measurements directly measure the quasiparticle dispersion and clearly resolve the Dirac cone with a Fermi velocity that is indistinguishable from that of single layer graphene. Despite a careful search, no evidence is found in these measurements for any type of hybridization between Dirac cones in the spectral regions where they cross [30]. The simplest interpretation of the ARPES data is that the first few graphene layers accessible to this spectroscopy are electronically floating, i.e. extremely weakly coupled to each other and to deeper layers in the film.

An important goal for theory in this area is therefore to identify situations where the effects of the interlayer coupling across a rotational fault are manifested in their electronic behavior. There has been progress in this direction. Bistritzer and MacDonald have studied the effect of the rotation angle of a bilayer on its interlayer tunneling conductance, predicting dramatic enhancements of the vertical conductance at special rotation angles that can be identified with low order commensurate superlattices [31]. More recent work has pointed to nontrivial effects of a θ-dependent interlayer coupling on the equilibrium charge redistribution across the bilayer in a perpendicular field [32]. Kindermann and I studied the Landau level spectra for weakly coupled bilayers and find that even a weak coherence splitting of bilayer bands at energies well above the mass scale produces a striking new effect, the Dirac comb [33]. Here small differences in the orbitally quantized states in two weakly coherence-split bands produces an amplitude modulation of the Landau level spectrum with a period that greatly exceeds the coherence scale, and should be observable by magnetotransport in the weak field regime. Small rotations angles can introduce long spatial Moire periods for twisted bilayers that can be made commensurate with the magnetic length $\sqrt{\hbar/eB}$ on accessible field scales, accessing Hofstadter commensuration physics in a new family of materials [34]. The band flattening theoretically predicted for in the small twist angle regime will surely focus attention on many body effects in the low energy physics. Further studies along all of these lines provide a very open area for further work.

One might be discouraged by the lack of a definitive theory of the electronic structure of rotationally faulted graphenes. To the contrary this is an exciting situation. These systems are challenging to the most familiar tools of electronic structure theory and their understanding is likely to involve creative new approaches.

Acknowledgements

References

[1] Novoselov K S, Geim A K, Morozov S V, Jiang D, Katsnelson M I, Grigorieva I V, Dubonos S V and Firsov A A 2005 *Nature* **438** 197

[2] Zhang Y, Tan Y-W, Stormer H L, and Kim P 2005 *Nature* **438** 2005

[3] McCann E and Fal'ko V 2006 *Phys. Rev. Lett.***96** 086805

[4] Koshino M and McCann E 2009 *Phys. Rev.* B **80** 165409

[5] Min H and MacDonald A H 2008 *Prog. Theor. Phys.* Suppl. No **175** 1

[6] Min H and MacDonald A H 2008 *Phys. Rev.* B **77** 155416

[7] Taychatanapat T, Watanabe K, Taniguchi T and Jarillo-Herrero P 2011 *Nature Physics* DOI:10.1038/nphys2008

[8] Berger C *et al.* 2006 *Science* **312** 1191

[9] de Heer W A, Berger C, Wu X, Sprinkle M, Hu Y, Ruan M, Stroscio J A, First P N, Haddon R, Piot B, Faugeras C, Potemksi and Moon J-S 2010 *J. Phys. D* **43** 374007

[10] Hass J, Varchon F, Millan-Otoya J E, Sprinkle M, Sharma N, de Heer W A, Berger C, First P N, Magaud L and Conrad E H 2008 *Phys. Rev. Lett.* **100** 125504

[11] Reina A *et al* 2009 *Nano Lett.* **9** 30

[12] Schmidt H, Ludtke T, Barthold P, McCann E, Fal'ko V I and Haug R I 2008 *Appl. Phys. Lett.* **93** 172108

[13] Li G and Andrei E Y 2007 *Nature Physics* **3** 623

[14] Li G, Luican A and Andrei E Y 2009 *Phys. Rev. Lett.* **102** 176804

[15] Miller D M, Kubista K D, Rutter G M, Ruan M, de Heer W A, First P N and Stroscio J A 2009 *Science* **324** 9242

[16] Sprinkle M *et al.* 2010 *Phys. Rev. Lett.* **81**, 155436 (2010)

[17] Lopes dos Santos J M B, Peres N M R and Castro Neto A H 2007 *Phys. Rev. Lett.* **99** 256802

[18] Li G, Luican A, Lopes dos Santos J M B, Castro Neto A H, Reina A, Kong J and Andrei E Y 2009 *Nature Physics* **6** 109

[19] Mele E J 2010 *Phys. Rev.* B **81** 161405

[20] Luican A, Li G, Reina A, Kong J, Nair R R, Novoselov K S, Geim A K and Andrei E Y 2011 *Phys. Rev. Lett* **106** 126802

[21] Latil S, Meunier V and Henrard L 2007 *Phys. Rev.* B **76** 201402

[22] de Laissardière G T, Mayou D and Magaud L 2010 *Nano Letters* **10** 804

[23] Shallcross S, Sharma S and Pankratov O A 2008 *Phys. Rev. Lett.* **101** 056803 (2008)

[24] Shallcross S, Sharma S, Kandelaki E and Pankratov O A 2010 *Phys. Rev.* B **81**, 1

[25] Bistritzer R and MacDonald A H 2011 *Proc. Nat. Acad. Sci.* **108** 12233

[26] Castro E V, Novoselov K S, Morozov S V, Peres N M R, Lopes dos Santos J M B, Nilsson J, Guineau F, Geim A K, and Castro Neto A H 2007 *Phys. Rev. Lett* **99** 216802

[27] de Gail R, Goerbig M O, Guinea F, Montambaux G, Castro Neto A H 2011 *Phys. Rev.* B **84** 045436

[28] Choi M-Y, Hyun Y-H and Kim Y 2011 *arXiv:1105.4551v1*

[29] Castro E V, Novoselov K S, Morozon S V, Peres N M R, Lopes dos Santos J M B, Nilsson J, Guinea F, Geim A K and Castro Neto A H 2010 *J. Phys.: Condes. Matter* **22** 1

[30] Hicks J *et al.* 2011 *Phys. Rev.* B **83** 205403

[31] Bistritzer R and MacDonald A H 2010 *Phys. Rev.* B **81** 245412

[32] Suarez Morelli E, Vargas P, Chico L and Brey L 2011 *arXiv*: 1108.0395v1

[33] Kindermann M and Mele E J 2011 *arXiv*:1106.0204

[34] Bistritzer R and MacDonald A H 2011 *Phys. Rev.* B **84** 035440